

The dynamical generation of two-dimensional matter-wave discrete solitons

Artem M Dudarev^{1,2,4}, Roberto B Diener^{1,3} and Qian Niu¹

¹ Department of Physics, The University of Texas, Austin, TX 78712, USA

² Center for Nonlinear Dynamics, The University of Texas, Austin, TX 78712, USA

³ Department of Physics, The Ohio State University, Columbus, OH 43210, USA

E-mail: dudarev@physics.utexas.edu

Received 31 October 2003, accepted for publication 3 March 2004

Published 4 May 2004

Online at stacks.iop.org/JOptB/6/S231

DOI: 10.1088/1464-4266/6/5/010

Abstract

We suggest a method to experimentally obtain two-dimensional matter-wave discrete solitons with a *self-repulsive* Bose–Einstein condensate in optical lattices. At the edge of the Brillouin zone, a wavepacket effective mass is negative, which could be treated as an inversion of the nonlinearity sign. Above critical nonlinearity this makes the wavepackets collapse partially into localized modes with a chemical potential located in the gap between the first and the second bands. This critical nonlinearity is also associated with the smallest nonlinearity for which the discrete solitons are possible in the gap. Extensive numerical simulations for square and asymmetric honeycomb lattices in the continuous model illustrate every stage of the process.

Keywords: discrete solitons, Bose–Einstein condensate, two-dimensional optical lattices

(Some figures in this article are in colour only in the electronic version)

1. Introduction

Periodic lattices with substantial nonlinearities appear in various systems such as biological molecules [1], nonlinear optical wave guides [2], solid-state materials [3, 4], and Bose–Einstein condensates (BECs) [5]. In these systems, interplay between linear coupling effects among adjacent sites and nonlinearity can result in a self-localized state—a lattice or ‘discrete’ soliton (DS) [1–5]. Until recently direct observation of DSs has been done only in one-dimensional (1D) optical wave guides [2, 6, 7]. Yet in systems with dimensionality more than one a number of fundamental phenomena, such as vortex lattice solitons, bright lattice solitons that carry angular momentum, are expected [8]. Recently a novel experimental technique to produce a photonic crystal with optical induction allowed the authors of [9] to directly observe two-dimensional (2D) DSs.

The dynamics of the optical pulses in nonlinear photonic crystals and BECs in optical lattices are governed by a nonlinear Schrödinger equation (NLSE) with periodic potential, hence many predictions done with respect to photonics are expected with BECs. In the case of BECs, the nonlinear coefficient can be either positive or negative for repulsive or attractive atomic interaction, respectively, with most of the experiments being done with repulsive atoms. One-dimensional solitons in the absence of periodic potential were observed in attractive BECs [10, 11]. One-dimensional matter-wave DSs in optical lattices were extensively studied theoretically both for attractive and repulsive interactions [12–14]. The decoherence of the repulsive BEC during Bloch oscillation in 1D optical lattices observed in experiments [15–17] was related theoretically to the generation of DSs [5, 18] (similar decoherence phenomena in two- and three-dimensional (3D) optical lattices have been reported [19, 20]). After the submission of this paper, the observation of the matter-wave DS was reported in 1D [21].

⁴ Author to whom any correspondence should be addressed.

In contrast to free space, stable localized modes are possible in periodic potentials in any dimension both for attractive and repulsive interaction. In the case of a *self-repulsive* BEC, the generation of multidimensional matter-wave DSs due to a modulational instability has been predicted theoretically [22], and the existence and stability of 2D DSs have been studied [23]. Using a variational approximation and direct numerical simulation the authors of [24] demonstrated that in the case of *attractive* interaction above the threshold number of atoms, the initial BEC wavepacket placed in an optical lattice collapses into multidimensional DSs.

The effect of the lattice for quantum wavepackets much larger than the unit cell of the periodic potential may be replaced by the effective mass. In which case, even for *repulsive* interaction, the wavefunction envelope dynamics, for points in momentum space where the effective mass is negative, are governed by the NLSE with negative (self-focusing) nonlinearity [25, 26]. The centre of the quantum wavepacket in momentum space can be easily shifted in a controlled manner by accelerating the lattice (for instance by chirping the relative detuning of the beams creating the lattice) as was demonstrated in early experiments with cold atoms [27] and later with BECs [28]. Recently, the effects of negative effective mass have been studied with ^{87}Rb condensates in one-dimensional optical lattices [29].

In 2D, above a critical value of the self-focusing nonlinearity the wavepacket collapses. The nonlinearity in the case of BECs is determined by the number of atoms, scattering length, effective mass in the lattice, and frequency of the transverse confinement. When the wavepacket size becomes comparable to the size of a unit cell the effective mass approximation breaks down. If the nonlinearity is close to that one for which the DS is supported by the band gap, part of the wavefunction is transferred to the DS and part decays into linear waves. This is a general phenomenon for the NLSE when a state is prepared sufficiently close to the localized state [30].

In this paper, we first obtain a criterion for the critical value of interaction using a variational approximation for the wavepacket envelope dynamics [31, 32] and effective mass approximation [25, 26]. We also show that this critical nonlinearity is comparable to the smallest nonlinearity for which the lattice supports DSs [33–35]. In the following section, we illustrate DS generation with a self-repulsive BEC using two numerical examples: a square optical lattice for the parameters considered in [23] and an asymmetric honeycomb lattice. The latter was originally considered as a system to study the effects of Berry curvature in periodic potentials [36]. For both systems, we simulate all the stages of the possible experiments: adiabatic introduction of the lattice, half of the Bloch oscillation, and waiting period for the wavefunction to collapse to DS. Finally, we summarize the results of this study.

2. Variational approximation

The variational approximation for the NLSE was originally developed in nonlinear optics (for a review see [32]). It was successfully applied to describe BEC dynamics [37–41], including its evolution in optical lattices [5, 24, 42]. In this section we first apply variational approximation ideas to the

evolution of the BEC Gaussian wavepacket in free space in D dimensions.

The Gross–Pitaevskii (GP) equation is an NLSE describing the dynamics of a BEC:

$$i\hbar \frac{\partial}{\partial t} \psi(\mathbf{r}, t) = \hat{H} \psi(\mathbf{r}, t) \\ = \left(-\frac{\hbar^2}{2m} \nabla^2 + V(\mathbf{r}) + Ng_D |\psi(\mathbf{r}, t)|^2 \right) \psi(\mathbf{r}, t), \quad (1)$$

with a nonlinear term being due to the mean-field treatment of the interaction between the atoms. It can be either positive and negative depending on the scattering length of the atomic collisions. Most of the current experiments deal with self-repulsive BECs (positive scattering length). The wavefunction in the equation is normalized to unity.

To apply variational approximation, we restrict the dynamics of the quantum wavepacket in free space ($V(\mathbf{r}) = 0$) in D dimensions to the form

$$\Psi_D(r) = \left(\frac{\alpha}{\pi} \right)^{D/4} e^{-(\alpha+i\beta)r^2/2}, \quad (2)$$

where α and β are variational parameters, α being inversely proportional to the width of the wavepacket squared. The semi-classical Lagrangian corresponding to the GP equation may be written as

$$L(\alpha, \dot{\alpha}, \beta, \dot{\beta}) = \langle \Psi_D | i\hbar \frac{\partial}{\partial t} - \hat{H} | \Psi_D \rangle. \quad (3)$$

The terms necessary for its calculation are

$$\langle \Psi_D | i\hbar \frac{\partial}{\partial t} | \Psi_D \rangle = \frac{\hbar D}{4} \frac{\dot{\beta}}{\alpha}, \quad (4)$$

$$\langle \Psi_D | -\frac{\hbar^2}{2M} \nabla^2 | \Psi_D \rangle = \frac{\hbar^2 D}{4m} \left(\alpha + \frac{\beta^2}{\alpha} \right), \quad (5)$$

$$V_{\text{int}} = \frac{Ng_D}{2} \int dr |\Psi_D(r)|^4 = \frac{Ng_D}{2} \left(\frac{\alpha}{2\pi} \right)^{D/2}. \quad (6)$$

The first term describes the temporal evolution, the second is associated with kinetic energy, and the last term describes the mean field interaction between particles. After the substitution $\gamma = 1/\alpha$ the Lagrangian equation becomes

$$\gamma \ddot{\gamma} - \frac{1}{2} \dot{\gamma}^2 = \frac{2\hbar^2}{m^2} + \frac{2Ng_D}{m} \gamma \left(\frac{1}{2\pi\gamma} \right)^{D/2}. \quad (7)$$

In the free space case, without mean field interaction ($g_D = 0$), this equation gives an exact result for the dependence of the wavepacket dispersion on time

$$\gamma^2 = 2(\sigma_0^2 + At^2), \quad (8)$$

where $\sigma_0^2 = \gamma^2(t=0)/2$ is the initial spatial second moment of the wavepacket, and

$$A = \frac{\hbar^2}{2m^2\gamma^2(t=0)} = \frac{\hbar^2}{4m^2\sigma_0^2}. \quad (9)$$

Equation (7) is particularly simple in 2D. In this case, the right-hand side becomes independent of parameters of the wavepacket, and the dynamics is effectively described in the same way as for non-interacting atoms. The wavepacket

becomes dispersionless when the right-hand side of (7) vanishes. This gives a criterion for the critical interaction strength

$$Ng_c = \frac{2\pi\hbar^2}{m}. \quad (10)$$

For negative nonlinearity, when $|g| > g_c$, the wavepacket collapses.

The quantum motion of a wavepacket in a periodic potential can be effectively described as motion in free space using the concept of effective mass, which in principle may be negative. We comment on this in the next section.

3. Effective mass

When the external potential $V(\mathbf{r})$ is periodic, and the size of the quantum wavepacket is much larger than its unit cell, the effect of the potential for different wavevectors \mathbf{k}_0 may be described in terms of the effective mass. This mass may be inferred from the band dispersion [25, 26]

$$m_{\text{eff},\mu\nu} = \hbar^2 \left(\frac{\partial^2 E}{\partial k_\mu \partial k_\nu} \right)^{-1}. \quad (11)$$

When the wavepacket is delocalized in real space over many lattice sites, in momentum space it is localized around a given wavevector \mathbf{k}_0 . In this case it may be represented as a sum of envelopes $f_n(\mathbf{r})$ over different Bloch bands

$$\psi(\mathbf{r}, t) = \sum_n f_n(\mathbf{r}, t) \phi_{n\mathbf{k}_0}(\mathbf{r}) e^{-iE_{n\mathbf{k}_0}t/\hbar}, \quad (12)$$

where the envelope $f_n(\mathbf{r}, t)$ is a slowly varying function within the unit cell, and each Bloch function $\phi_{n\mathbf{k}_0}$ is the solution of the linear eigenproblem

$$\left(-\frac{\hbar^2}{2m} \nabla^2 + V(\mathbf{r}) \right) \phi_{n\mathbf{k}}(\mathbf{r}) = E_{n\mathbf{k}} \phi(\mathbf{r}), \quad (13)$$

normalized to the area of the unit cell

$$\int_{\text{cell}} d\mathbf{r} |\phi_{n\mathbf{k}_0}(\mathbf{r})|^2 = \Omega. \quad (14)$$

In experiments it is possible to prepare wavepackets that populate only the lowest band [27]. The NLSE for the envelope incorporates the effects of the external potential into effective mass [25, 26]

$$i\hbar \left(\frac{\partial f_n}{\partial t} + \mathbf{v}_g \cdot \nabla f_n \right) = \left(-\frac{\hbar^2}{2m_{\text{eff},\mu\nu}} \frac{\partial^2}{\partial x_\mu \partial x_\nu} + Ng'_2 |f_n|^2 \right) f_n, \quad (15)$$

where \mathbf{v}_g is the drift velocity of the wavepacket centre

$$\mathbf{v}_g = \frac{1}{m} \langle \phi_{n\mathbf{k}_0} | \hat{\mathbf{p}} | \phi_{n\mathbf{k}_0} \rangle, \quad (16)$$

and the effective interaction strength g'_2 is given by

$$g'_2 = \frac{g_2}{\Omega} \int_{\text{cell}} d\mathbf{r} |\phi_{n\mathbf{k}_0}(\mathbf{r})|^4. \quad (17)$$

In the particular examples we will discuss below, the wavepacket will be driven to the point in the Brillouin zone

where $\mathbf{v}_g = 0$, and the effective mass tensor is negative in all directions; hence the envelope dynamics will be governed by an NLSE with negative mass. This can be viewed as an NLSE with *positive* mass with *inverted* sign of nonlinearity, which is clearly seen from the equation for the complex conjugate of the envelope function

$$i\hbar \frac{\partial f_n^*}{\partial t} = \left(-\frac{\hbar^2}{2|m_{\text{eff},\mu\nu}|} \frac{\partial^2}{\partial x_\mu \partial x_\nu} - Ng'_2 |f_n^*|^2 \right) f_n^*. \quad (18)$$

This equation can be obtained by taking the complex conjugate of (15) and using the absolute value of the mass.

Hence, in this situation, as long as the condition for the effective mass approximation holds, m in equation (7) should be replaced by m_{eff} . In the case when an effective mass and nonlinearity have opposite signs and $|g'_2| > g'_{2,c}$, where the critical interaction strength is defined in (10), with mass being replaced by effective mass, the wavepacket collapses. Notice that in general from (7) it follows that the dispersion of the wavepackets for any D when the effective mass is negative is described by the equation with positive mass and inverted sign of nonlinearity. When the size of the wavepacket becomes comparable to the lattice spacing, the effective mass approximation no longer holds. As we will discuss in the following section, in 2D there is nonlinearity below which the DSs are not supported by the bandgap. If the nonlinearity is sufficiently larger than this delocalizing nonlinearity, part of the wavepacket decays into DSs and part decays into linear waves.

4. Delocalization

In contrast to 1D, where DSs may correspond to arbitrary nonlinearity, in 2D and higher dimensions DSs are possible only for nonlinearity above a critical value [33]. The authors of [34] considered the possibility of observing the delocalization transition with matter-wave DSs in optical lattices, when an irreversible change from DSs to delocalized states is produced for a slow change in the lattice parameters. This delocalizing nonlinearity may be associated with the critical nonlinearity for a Gaussian wavepacket to collapse, as discussed in section 2.

The concept of the effective mass is not generally applied to the DS since in the middle of the gap the DS is localized within one lattice site. As the chemical potential of the DS comes close to a band of linear states, its space extension increases; hence one may expect that the effective mass approximation becomes applicable. The results of section 2 imply that there is only one value of nonlinearity for which the localized modes are supported in 2D free space when the envelopes of the localized modes are approximated by Gaussians. This also can be shown in general from the scaling arguments for the 2D NLSE. Indeed, if the normalized wavefunction $\psi_1(x, y)$ is the solution of

$$-\nabla^2 \psi_1 + \gamma \psi_1^3 = \tilde{\mu} \psi_1, \quad (19)$$

then the normalized wavefunction $\psi_2 = B\psi_1(Ax, Ay)$ is the solution of

$$-\nabla^2 \psi_2 + \gamma \psi_2^3 = A^2 \tilde{\mu} \psi_2. \quad (20)$$

This means that in 2D free space there is only one possible value of γ for which localized modes can be found for any value of $\tilde{\mu}$.

Localized wavepackets with very large extension correspond to the critical nonlinearity. As their size is reduced, other corrections due to the lattice also start to play a role. The variational approximation gives a clear picture of what happens to initially localized states of the NLSE in 2D. It predicts the critical value of nonlinearity above which the evolution of the wavepacket width changes character. One may expect that the value of Ng_c given in (10) is close to the exact one. We confirmed this expectation by performing direct self-consistent numerical simulations based on the effective potential approach suggested in [35]. Similar to the self-consistent Hartree–Fock approximation, one may consider a DS to be a localized state in the effective potential created by itself:

$$V_{\text{eff}}(\mathbf{r}) = -Ng'_D |\psi(\mathbf{r})|^2. \quad (21)$$

In the numerical simulation, we started with an *arbitrary* nodeless initial wavefunction, and with imaginary time evolution found the ground state of the potential (21) for the Hamiltonian given by

$$\hat{H}_{\text{eff}} = -\frac{\hbar^2}{2|m_{\text{eff}}|} \nabla^2 + V_{\text{eff}}(\mathbf{r}), \quad (22)$$

and used it in the next step of the iteration. We found that independent of the initial guess state above the critical value

$$Ng'_{\text{num}} = \frac{5.850 \hbar^2}{|m_{\text{eff}}|}, \quad (23)$$

the self-consistent procedure resulted in collapsing states with infinite negative energy, while for smaller nonlinearities the states expanded, with energy going to zero. This value differs from the one for an extended Gaussian wavepacket to collapse (10) by $\sim 10\%$.

As an alternative method we also reduced the 2D equation to a 1D ordinary differential equation and solved the two point boundary value problem ($\psi'(0) = 0$, $\psi(\infty) = 0$) with the shooting method [43]. We found that for arbitrary energy, nodeless solitons in free space with arbitrary size are supported only for one value of nonlinearity given by the same value as in (23).

The direct dynamical simulations discussed in the next section confirm the existence of the critical nonlinearity above which a wavepacket with a finite size collapses. Also, using imaginary time evolution for different values of chemical potential in the gap, we find a corresponding nonlinearity for DSs in the lattice to exist. The minimum nonlinearity found as a result of this calculation is comparable to (10) and (23).

5. Numerical simulations

5.1. General remarks

By choosing appropriate units of length, L_u , and mass, $M_u = M_{\text{atom}}$, the GP equation (1) is reduced to a dimensionless form:

$$i \frac{\partial \psi}{\partial t} = \left[-\frac{1}{2} \nabla^2 + V_L(\mathbf{r}) + Ng_2 |\psi|^2 + \mathbf{F} \cdot \mathbf{r} \right] \psi. \quad (24)$$

We also add an external force \mathbf{F} that in the case of optical lattices may be created by accelerating the lattice, for example, by sweeping the relative frequency of the beams creating the lattice. In this case, the unit of energy of the problem is $E_u = \hbar^2/M_u L_u^2$ and the unit of time is given by $t_u = \hbar/E_u$. When the unit of length is chosen to be equal to the inverse wavevector of the light creating the optical lattice $L_u = 1/k_L$, typical maximum depths of the optical potentials achievable in the dissipationless regime are ~ 20 . The forces created by accelerating the lattice are limited due to the finite lifetime of the excited states: in the case of alkali atoms to about 1000; in experiments [27] forces of the order of ~ 1 – 10 were used. The dynamics of the BEC is described by a 2D equation in the case when the strong confinement in the transverse direction ‘freezes’ the wavefunction in that direction to the harmonic oscillator ground state. This happens when the oscillator length in that direction ($l_z = \sqrt{\hbar/M_{\text{atom}}\omega_z}$) becomes smaller than the condensate healing length $\xi = (4\pi n a)^{-1/2}$, where n is the atomic density and a is the scattering length. When, at the same time, l_z is still larger than the 3D scattering length, $|a|$,

$$|a| < l_z < \xi, \quad (25)$$

the collisions between the atoms preserve their 3D character, yet the dynamics of the BEC in the two other directions are effectively described by a 2D GP equation [44]. Such a regime was recently demonstrated experimentally [45]. The nonlinear coefficient in this case is given by

$$g_2 = \left(\frac{8\pi\omega_z \hbar^3}{M_{\text{atom}}} \right)^{1/2} a. \quad (26)$$

The experimental system, therefore, provides great flexibility with which the nonlinear coefficient in the corresponding NLSE can be controlled. Parameters that are variable in experiments are the number of atoms, N , the frequency of transverse confinement ω_z , and the scattering length, a , that in principle may be tuned by a magnetic field with Feshbach resonances [46]. For the experimental parameters of [45] we estimate the nonlinear coefficient in present units to be $Ng_2 \sim 6000$. For the ansatz chosen above to be a good choice, the kinetic energy (5) should be larger than the interaction energy (6). This means that the nonlinearity should be smaller than $\sim 2\pi$. Below we consider only the cases when this holds. For a BEC the effective nonlinearity can always be reduced by changing either the number of atoms or the trapping frequency in the transverse direction.

The stationary states of equation (24) are described by solutions in the form $\psi(\mathbf{r}, t) = \phi(\mathbf{r}) \exp(-i\mu t)$, where μ is the chemical potential. Localized states can be found for μ in the gaps of the linear problem.

Below, we consider two examples. The first one is based on parameters for which the existence and stability of the solitons were studied in [23]. Our consideration extends the treatment to suggest a specific approach for DS generation based on the ideas outlined in previous sections. The second example deals with the asymmetric honeycomb lattice that was studied by us [36] in the context of observing self-rotation and Berry curvature effects for quantum wavepackets in asymmetric periodic potentials. There, robust spontaneous generation of the DS above a critical interaction strength was

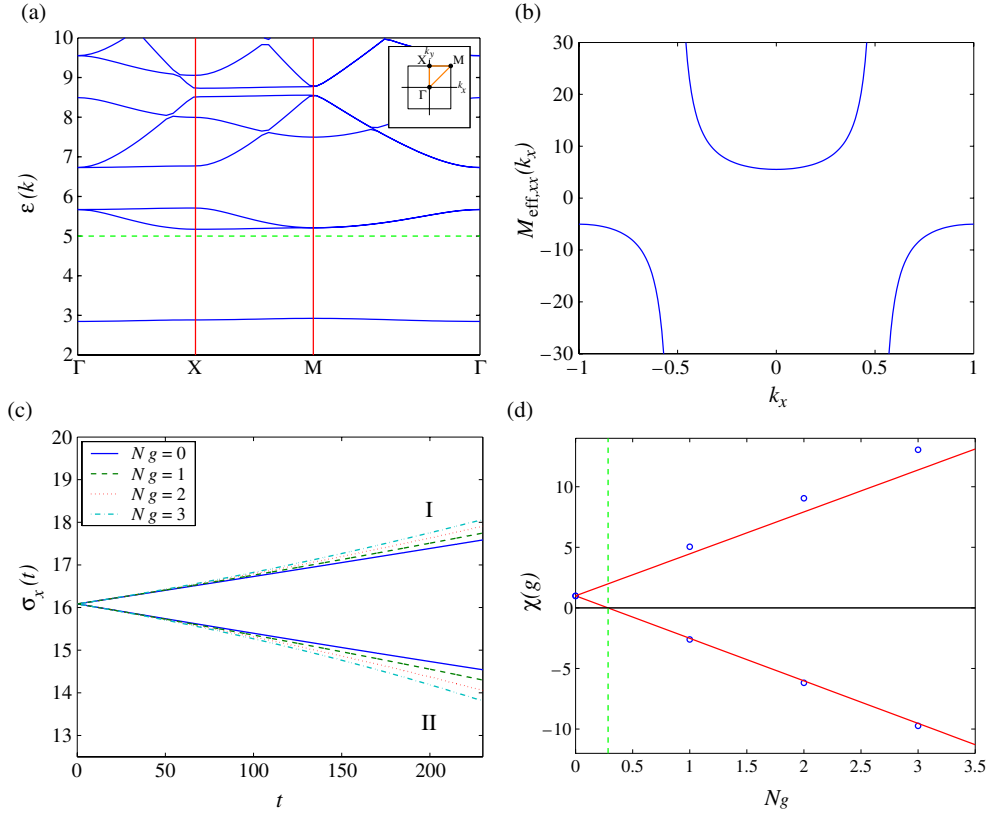


Figure 1. (a) The dispersion for a square lattice potential (31) along the high symmetry path. The dashed line shows the boundary between strongly bound and quasi-unbound states [23]. (b) The xx component of the effective mass tensor along the k_x -axis. (c) The dependence of wavepacket dispersion on time after the lattice potential is introduced. The two sets of curves are for different points in the Brillouin zone: (I) point Γ , (II) point M. (d) The dispersive characteristic χ from (39). The dots are obtained from fitting quadratic dispersion (8) to continuous simulation data from panel (c); the line is the expected behaviour of χ .

observed for wavepackets left at the corner of the Brillouin zone. Here, we discuss how this effect could be naturally explained in terms of the effective mass concept.

In both cases we have performed simulations in a form that mimics possible experiments. We start with a Gaussian wavepacket in free space with a size that is much larger than the unit cell of the potential. The process may be divided into three stages: (1) adiabatic introduction of the lattice potential, (2) acceleration of the lattice for half of the Bloch oscillation, and (3) a waiting period for the wavepacket to collapse. In the first two stages, adiabaticity is crucial. An adiabatic criterion can be estimated based on the Landau–Zener formalism for tunnelling between two levels with an avoided crossing. In this case the probability to tunnel is given by [47, 48]

$$P = \exp\left(-\frac{\pi \delta^2}{2\alpha}\right), \quad (27)$$

where δ is the gap between the states and α is the rate of change of the gap. This criterion, when a periodic potential with amplitude V_0 is introduced in time t_V , becomes

$$\frac{\delta^2 t_V}{V_0} \gg 1, \quad (28)$$

where δ is the gap between the first and the second bands at $k = 0$, since originally the width of the wavepacket in momentum space is much smaller than the size of the Brillouin

zone (note that units with $\hbar = 1$ are used). The maximum ‘force’ of the drive may be similarly estimated as

$$\frac{\epsilon_g}{\frac{\partial \epsilon}{\partial k} F} \gg 1. \quad (29)$$

Here ϵ_g is the smallest gap between the first and the second bands, and $\partial \epsilon / \partial k$ is the largest slope of the dispersion. An alternative expression may be derived based on the WKB approximation [49]:

$$\frac{\epsilon_g^{3/2} m_{\text{eff}}^{1/2}}{F} \gg 1 \quad (30)$$

where the effective mass, m_{eff} , can be estimated from the dispersion as well. We made sure that the adiabaticity criteria are fulfilled in the simulations discussed below. We also checked it numerically by increasing the driving force and observing the breakdown of the adiabaticity.

5.2. Square lattice

As a first example, we discuss the model potential considered in [23] for the existence and stability of 2D DSs in continuous potentials, namely

$$V_L(x, y) = V_0(\sin^2 x + \sin^2 y). \quad (31)$$

Such a potential may be experimentally obtained by overlapping two pairs of counter-propagating beams, far

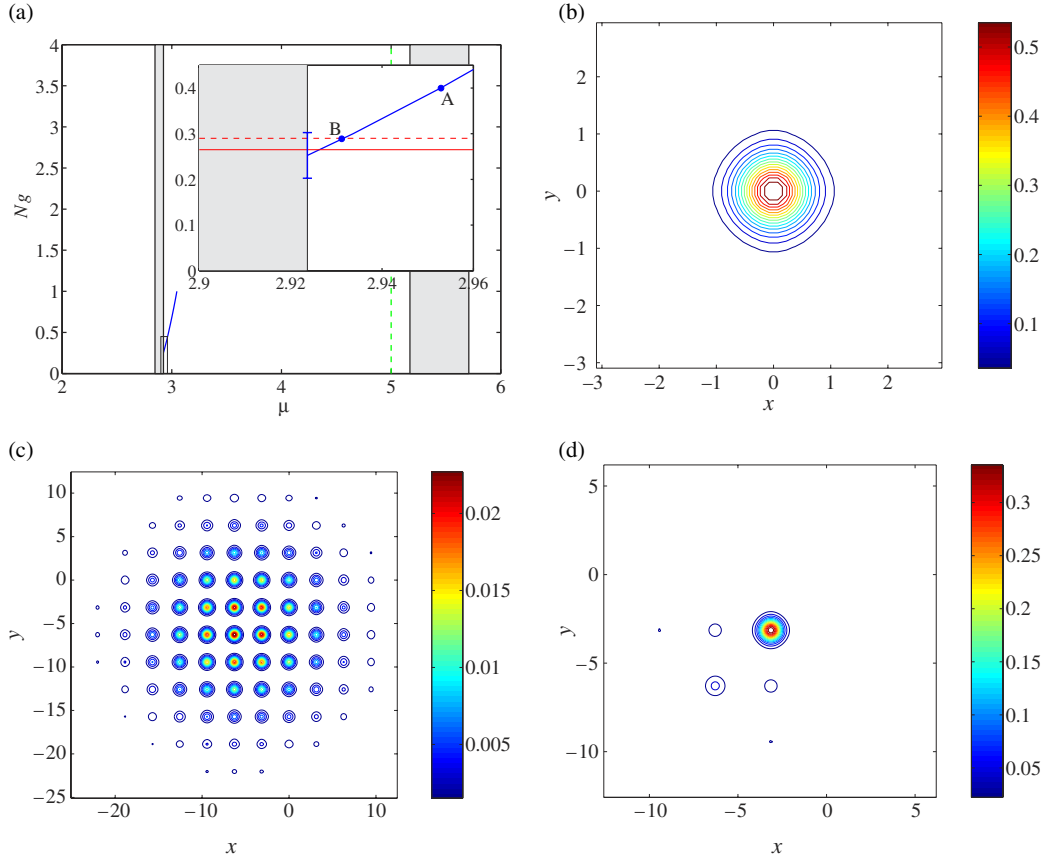


Figure 2. (a) The dependence of nonlinearity on the corresponding chemical potential. The first and second bands are shown with solid rectangles. The inset shows a region denoted by a rectangle in the lower left-hand corner. The horizontal solid line shows the numerical value for delocalizing nonlinearity, g_{num} ; the dashed line is the critical nonlinearity for the extended Gaussian wavepacket to collapse, $g_{2,c}$. (b) The spatial distribution of DSs corresponding to $\mu = 0.7$ obtained with the descent method. (c) The probability distribution for the BEC wavefunction evolved with $Ng_2 = 0.2$ for $\Delta t \sim 1500$ after it was driven to the M point. (d) The same for $Ng = 0.4$ (point A in (a)); approximately 0.72 of the wavefunction probability is transferred to the soliton, which corresponds to an effective nonlinearity of $Ng_{2,\text{eff}} \approx 0.288$ —at the top of the first band (point B in (a)).

detuned from atomic resonance to reduce the effects of spontaneous emission. As in [23], we use amplitude $V_0 = 5$.

In figure 1(a), we show the dispersion of the linear problem (13) for the potential (31) along the high symmetry directions. The first band has a minimum at zero momentum (Γ point), and a maximum at the corner of the Brillouin zone (M point). There exist directions on the plane for which the maximum value of the potential is smaller than V_0 . These are orthogonal (x, y) directions, while the absolute maximum of the potential is $2V_0$. For the chemical potential of the localized states above V_0 (shown as a dashed line in figure 1(a)), the BEC states are quasi-unbound. For values of μ close to this boundary an adequate description of DSs is not possible within the one-band tight-binding model. This is because situations when nodes of the solitonic wavefunctions are located at the potential minima are possible [23].

The xx -component of the effective mass tensor (11) is shown in figure 1(b). Since the potential is separable and symmetric, the yy -component has the same dependence on k_y , and the tensor is diagonal. At the points of global maximum and minimum of the dispersion, the effective mass in both directions is the same. At the Γ point, the effective mass has the smallest positive value ($m_{\text{eff},\Gamma} = 5.53$), while at the point M it is negative and has the smallest absolute value ($m_{\text{eff},M} =$

-5.03). Hence the smallest nonlinearity is necessary for the wavepacket to self-collapse at the M point. The fact that in 1D, for a sinusoidal potential for wavevectors, k , larger than half of the largest vector in the Brillouin zone, $k > k_{\text{crit}} = \pi/(2a)$, where a is the lattice spacing, allows us to give a physical explanation of the origin of the Landau instability studied in [50] in terms of tight-binding approximation. For any interaction strength, wavepackets composed of Bloch waves for $k < k_{\text{crit}}$ remain wavepackets composed of Bloch waves, while for $k > k_{\text{crit}}$, when interaction is large enough, they partially collapse to localized modes.

To investigate the validity of the effective mass description, we checked in numerical simulations the predictions that may be based on the formulae discussed in the previous sections. From (9), we introduce the quantity characterizing the dispersion of the wavepacket

$$\chi = \frac{A\sigma^2}{A\sigma^2|_{g_2=0}} = 1 + \frac{Ng'_2 m_{\text{eff}}}{2\pi}, \quad (32)$$

which changes linearly with the interaction. As it becomes negative, the wavepacket collapses. Notice that in this expression the effective interaction strength is related to the continuous interaction strength with (17), which for the case

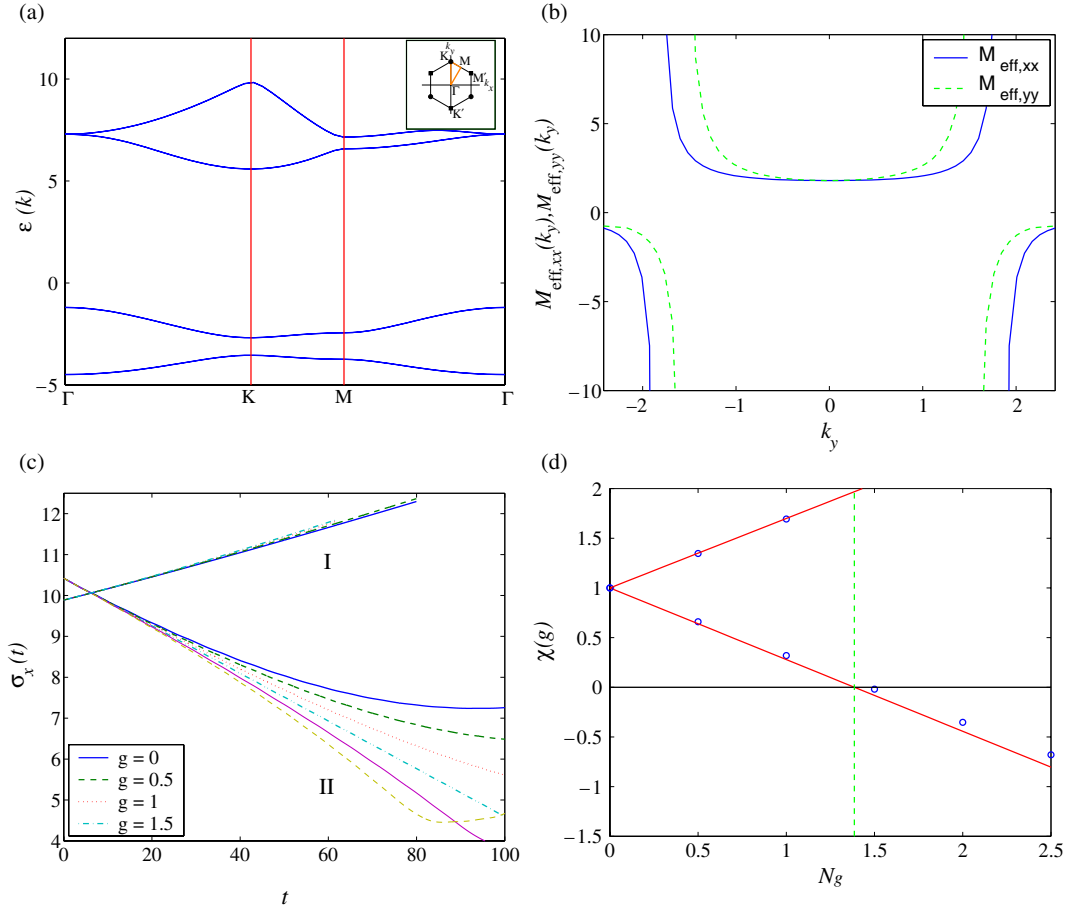


Figure 3. (a) The dispersion for the asymmetric honeycomb potential (41) along a high symmetry path. The dashed line shows the boundary between strongly bound and quasi-unbound states [23]. (b) The xx and yy components of the effective mass tensor along the k_y -axis. (c) The dependence of the wavepacket dispersion on time after the lattice potential is introduced. The two sets of curves are for different points in the Brillouin zone: (I) point Γ , (II) point K. (d) The dispersive characteristic χ from (39). The dots are obtained from fitting the quadratic dispersion (8) to continuous simulation data from panel (c); the line is the expected behaviour of χ .

of separable sinusoidal potential at least partially may be computed analytically. For the separable potential (31) the solution of the stationary eigenproblem (13) is separable: $\phi(x, y) = \phi_x(x)\phi_y(y)$, where each wavefunction is given by the solution of the corresponding equation:

$$\left[\frac{1}{2} \frac{\partial^2}{\partial x^2} + \left(E - \frac{V_0}{2} \right) + \frac{V_0}{2} \cos 2x \right] \phi_x(x) = 0. \quad (33)$$

Due to Bloch–Floquet theorem, the solution is a product of a periodic Bloch function $u_k(x)$ and a plane wave:

$$\psi_{x,k_x}(x) = e^{ik_x x} u_k(x). \quad (34)$$

After the following substitutions

$$\begin{aligned} b &= 2 \left(E - \frac{V_0}{2} \right), \\ z &= x, \\ q &= -\frac{V_0}{2}, \\ \psi_x(x) &= y(z), \end{aligned} \quad (35)$$

equation (33) becomes the Mathieu equation [51]:

$$\frac{\partial^2 y}{\partial z^2} + (b - 2q \cos 2z)y = 0, \quad (36)$$

and as a result the solution of (33) gives Mathieu functions with characteristic value b and parameter q :

$$\psi_{x,k_x}(x) = \text{Ce}(b, q, z) = \text{Ce} \left(2 \left(E - \frac{V_0}{2} \right), -\frac{V_0}{2}, x \right). \quad (37)$$

Introducing the numerical factor

$$I = \frac{\left(\int_{-\pi/2}^{\pi/2} \text{Ce}_r^4(a, q, z) dz \right)^2}{\left(\int_{-\pi/2}^{\pi/2} \text{Ce}_r^2(a, q, z) dz \right)^4} \quad (38)$$

we get the following dependence of χ on the interaction strength:

$$\chi = 1 + \frac{\Omega m_{\text{eff}} I}{2\pi} Ng_2. \quad (39)$$

Therefore the critical interaction strength is given by

$$Ng_{2,c} = \frac{2\pi}{\Omega |m_{\text{eff}}| I}. \quad (40)$$

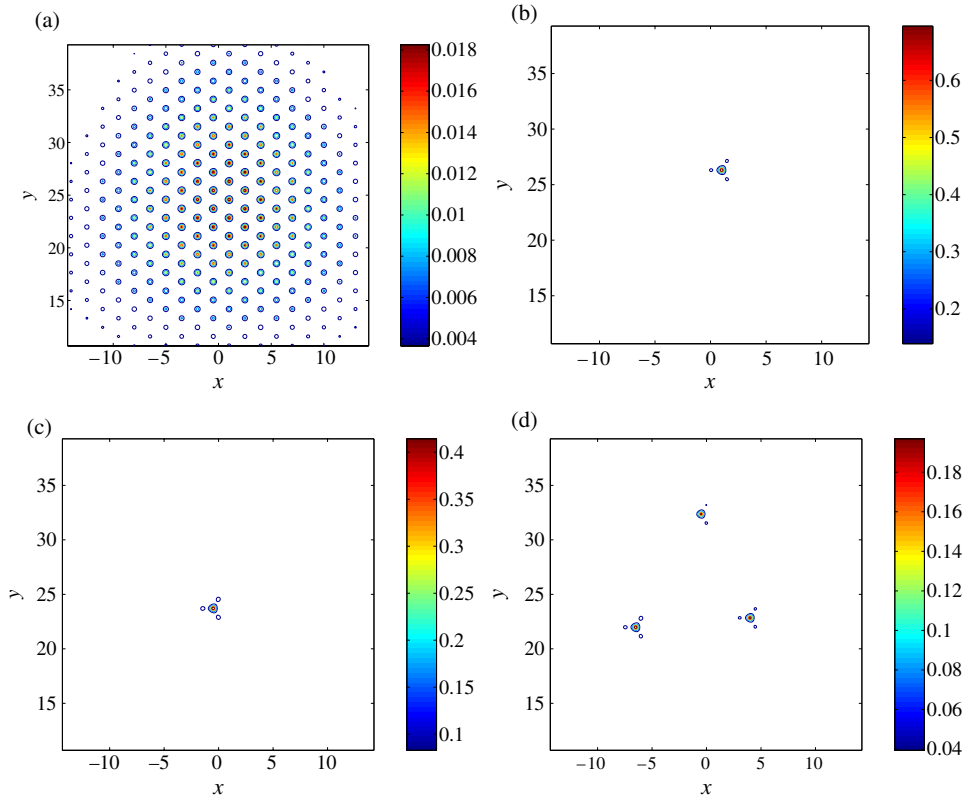


Figure 4. The probability density of the wavepacket that has been driven to the K point of a square lattice after expansion for $\Delta t_{\text{exp}} = 200$ with different interactions: (a) $Ng_2 = 0.5$, (b) $Ng_2 = 2.5$, (c) $Ng_2 = 5$ and (d) $Ng_2 = 10$. As the interaction increases, the fraction of the wavefunction transferred to solitons decreases.

For the considered example, the area of the lattice unit cell is $\Omega = \pi^2$ and the numerical factor for the top of the band is $I_M = 0.398$, which makes the critical interaction strength $Ng_{2,c} = 0.285$.

To test the predicted behaviour of the parameter ξ , we perform a numerical simulation with a continuous potential. We start with a wavepacket of size $\sigma_{x,y} = 15/\sqrt{2}$, while the size of the unit cell is π in each direction. The lattice potential is ramped from $V_0 = 0$ to 5 in $t_V = 450$, then the lattice is accelerated with force $F = 0.01$ in the diagonal [11] direction. The acceleration is halted after the wavepacket undergoes half of the Bloch oscillation; in other words, when its centre is located at point M in momentum space. After this, the wavepacket expands freely in the presence of the lattice potential. The ramp time and the force satisfy the adiabaticity conditions (28)–(30), so that the wavepacket during evolutions stays in the first band. In addition to expanding the wavepacket at the top of the band, we have studied the expansion as soon as the lattice was introduced without introducing an external field, \mathbf{F} . In both cases the agreement with the analytic prediction (32) is very good (see figures 1(c) and (d)).

As the external force is removed, the wavepacket contracts due to phases accumulated during the acceleration even in the linear case. But it is only when the interaction is above a critical condition that the localized modes are formed. To find a stationary localized solution we followed the optimization procedure based on a descent technique with Sobolev preconditioning used in [23] and described in [52]. In figure 2(a) we display the dependence of the nonlinearity on the

chemical potential of the DS. The error bar shows the estimated uncertainty for the curve to intersect the band of extended states obtained by interpolating to infinite size and infinite relaxation time of the descent procedure. The agreement with the argument based on effective mass and free space solitons given in section 4 is very good. As one starts with an extended wavepacket and nonlinearity supported by the gap, it shrinks and may lose some part to radiation (extended states), so that the effective interaction experienced by the localized mode is then just a fraction of the actual interaction. As shown in figure 2, the solitons are formed inside the gap. When the nonlinearity increases, their chemical potential increases but not significantly, so that they stay relatively close to the top of the first band.

5.3. Asymmetric honeycomb lattice

In our previous work [36] dedicated to study of quantum wavepacket propagation in spatially asymmetric optical lattices above a critical interaction strength, we have observed the self-collapse of the wavepacket into localized modes. The effective mass concept provides an explanation of the phenomena and relates the critical interaction strength to other parameters of the problem. Here, we describe briefly the model potential. The potential used in [36] is

$$V_{\text{lat}}(\mathbf{r}) = \sum_{i=1}^6 A_i \cos(\mathbf{k}_i \cdot \mathbf{r} + \phi_i), \quad (41)$$

with the following parameters:

$$\begin{aligned} A_1 &= A_3 = A_5 = -4, \\ A_2 &= A_4 = A_6 = -4.664, \\ \phi_1 &= \phi_3 = \phi_5 = 0, \\ \phi_2 &= -\phi_4 = \phi_6 = 1.1. \end{aligned} \quad (42)$$

It may be obtained either with interference of three pairs of counter-propagating beams or by holographic techniques. The band structure is shown in figure 3(a). Asymmetry splits the first band in the middle. In this case, the boundary between strongly bound and quasi-unbound states is located in the second gap. The effective mass is negative in both directions at the K point (see figure 3(b)). We start with a Gaussian wavepacket in free space which has spatial dispersion $\sigma_{x,y} = 10/\sqrt{2} \approx 7.071$. Since the size of the unit cell in this case is $\Omega = 3\sqrt{3}/2$, the wavepacket occupies several unit cells. The lattice potential is introduced in time $t_V = 120$ and we accelerate it along the y -axis with $|\mathbf{F}| = 0.05$. In this case the conditions in (28)–(30) are fulfilled. An analysis of the expansion for different values of the interaction at the bottom of the first band (Γ point) and the top of the first band (K point) is shown in the figure 3(c). To compare the results of the continuous simulation with the prediction of (32) we calculated the effective mass, M_{eff} , from the band structure and the numerical factor I , which involves integrals of the Bloch wavefunctions, by integrating over one unit cell the wavefunctions obtained by adiabatic evolution. Their values are $M_{\text{eff},\Gamma} = 1.7986$, $I_\Gamma = 0.9396$ at the point Γ and $M_{\text{eff},K} \approx -0.8918$, $I_K \approx 1.9567$ at the point K. Probability density plots after expansion for $\Delta t_{\text{exp}} = 200$ at the K point are shown in figure 4. As the interaction increased past the critical interaction the lattice solitons were dynamically formed. The figure illustrates that the phenomenon is also observed for a square lattice: the fraction of the wavefunction transferred to the localized modes decreases as the interaction strength is increased. The effective interaction experienced by each mode is such that the corresponding chemical potential is close to the first band.

As we have seen in the numerical examples discussed above, if the nonlinearity is small enough, the wavepacket collapses into a single DS. Clouds of ultracold atoms can be imaged non-destructively [53]. Observation of a persistent atomic cloud localized to dimensions comparable to the wavelength of the light forming the lattice is a clear sign of DS formation. Observation of the predicted delocalizing transitions with a single DS prepared in a controlled fashion for a varying lattice depth is also an exciting possibility.

6. Conclusion

In this paper we have shown how DSs could be generated with a self-repulsive BEC in optical lattices by driving the wavepackets to the points where the effective mass is negative, which leads to self-collapse of the wavepacket. As a result, part of the wavefunction is transferred to localized modes with chemical potential in between the first and second bands where DSs with positive nonlinearity are supported. In 2D, this happens only when the critical nonlinearity is achieved.

As the strength of the interaction increases, the wavepacket may excite several localized modes. We have observed that the effective interaction of each mode is such that the corresponding chemical potential is located close to the top of the first band.

Acknowledgments

We acknowledge support from the NSF and the R A Welch Foundation, and discussions with J Hanssen, K C Henderson, T P Meyrath, S A Moore and M G Raizen.

References

- [1] Davydov A S and Kislukha N I 1973 *Phys. Status Solidi* **b 59** 465
- [2] Christodoulides D N and Joseph R I 1988 *Opt. Lett.* **13** 794
- [3] Su W P, Schieffer J R and Heeger A J 1979 *Phys. Rev. Lett.* **42** 1968
- [4] Sievers A J and Takeno S 1988 *Phys. Rev. Lett.* **61** 970
- [5] Trombettoni A and Smerzi A 2001 *Phys. Rev. Lett.* **86** 2353
- [6] Eisenberg H S, Silberberg Y, Morandotti R, Boyd A R and Aitchison J S 1998 *Phys. Rev. Lett.* **81** 3383
- [7] Morandotti R, Peschel U, Aitchison J S, Eisenberg H S and Silberberg Y 1999 *Phys. Rev. Lett.* **83** 2726
- [8] Malomed B A and Kevrekidis P G 2001 *Phys. Rev. E* **64** 026601
- [9] Fleischer J W, Segev M, Efremidis N K and Christodoulides D N 2003 *Nature* **422** 147
- [10] Strecker K E, Partridge G B, Truscott A G and Hulet R G 2002 *Nature* **417** 150
- [11] Khaykovich L, Schreck F, Ferrari G, Bourdel T, Cubizolles J, Carr L D, Castin Y and Salomon C 2002 *Science* **296** 1290
- [12] Carusotto I, Embriaco D and La Rocca G C 2002 *Phys. Rev. A* **65** 053611
- [13] Louis P J Y, Ostrovskaya E A, Savage C M and Kivshar Y S 2003 *Phys. Rev. A* **67** 013602
- [14] Ahufinger V, Sanpera A, Pedri P, Santos L and Lewenstein M 2003 *Preprint* cond-mat/0310042
- [15] Anderson B P and Kasevich M A 1998 *Science* **282** 1686
- [16] Burger S, Cataliotti F S, Fort C, Minardi F, Inguscio M, Chiofalo M L and Tosi M P 2001 *Phys. Rev. Lett.* **86** 4447
- [17] Morsch O, Müller J H, Cristiani M, Ciampini D and Arimondo E 2001 *Phys. Rev. Lett.* **87** 140402
- [18] Scott R G, Martin A M, Fromhold T M, Bujkiewicz S, Sheard F W and Leadbeater M 2003 *Phys. Rev. Lett.* **90** 110404
- [19] Greiner M, Bloch I, Mandel O, Hänsch T W and Esslinger T 2001 *Phys. Rev. Lett.* **87** 160405
- [20] Greiner M, Mandel O, Esslinger T, Hänsch T W and Bloch I 2002 *Nature* **419** 51
- [21] Eiermann B, Anker Th, Albiez M, Taglieber M, Treutlein P, Marzlin K P and Oberthaler M K 2004 *Preprint* cond-mat/0402178
- [22] Baizakov B B, Konotop V V and Salerno M 2002 *J. Phys. B: At. Mol. Opt. Phys.* **35** 5105
- [23] Ostrovskaya E A and Kivshar Yu S 2003 *Phys. Rev. Lett.* **90** 160407
- [24] Baizakov B B, Malomed B A and Salerno M 2003 *Europhys. Lett.* **63** 642
- [25] Steel M J and Zhang W 1998 *Preprint* cond-mat/9810284
- [26] Pu H, Baksmaty L O, Zhang W, Bigelow N P and Meystre P 2003 *Phys. Rev. A* **67** 043605
- [27] Raizen M, Salomon C and Niu Q 1997 *Phys. Today* **50** (7) 30
- [28] Denschlag J H, Simsarian J E, Häffner H, McKenzie C, Browaeys A, Cho D, Helmerson K, Rolson S L and Phillips W D 2002 *J. Phys. B: At. Mol. Opt. Phys.* **35** 309

- [29] Eiermann B, Treutlein P, Anker Th, Albiez M, Taglieber M, Marzlin K-P and Oberthaler M K 2003 *Phys. Rev. Lett.* **91** 060402
- [30] Soffer A and Weinstein M I 2003 *Preprint nlin.PS/0308020*
- [31] Desaix M, Anderson D and Lisak M 1991 *J. Opt. Soc. Am. B* **8** 2082
- [32] Malomed B A 2002 *Prog. Opt.* **43** 71
- [33] Flach S, Kladko K and MacKay R S 1997 *Phys. Rev. Lett.* **78** 1207
- [34] Kalosakas G, Rasmussen K O and Bishop A R 2002 *Phys. Rev. Lett.* **89** 030402
- [35] Baizakov B B and Salerno M 2004 *Phys. Rev. A* **69** 013602
- [36] Diener R B, Dudarev A M, Sundaram G and Niu Q 2003 *Preprint cond-mat/0306184*
- [37] Carr L D and Castin Y 2002 *Phys. Rev. A* **66** 363602
- [38] Abdullaev F Kh, Caputo J G, Kraenkel R A and Malomed B A 2003 *Phys. Rev. A* **67** 013605
- [39] Perez-Garcia V M, Konotop V V and Garcia-Ripoll J J 2000 *Phys. Rev. E* **62** 4300
- [40] Tsurumi T and Wadati M 2001 *J. Phys. Soc. Japan* **70** 1512
- [41] Salasnich L, Parola A and Reatto L 2002 *Phys. Rev. A* **65** 043614
- [42] Abdullaev F Kh, Baizakov B B, Darmanyan S A, Konotop V V and Salerno M 2001 *Phys. Rev. A* **64** 043606
- [43] Press W H, Teukolsky S A, Vetterling W T and Flannery B P 1992 *Numerical Recipes in C* 2nd edn (Cambridge: Cambridge University Press) chapter 17
- [44] Petrov D S, Holzmann M and Shlyapnikov G V 2000 *Phys. Rev. Lett.* **84** 2551
- [45] Görlitz A, Vogels J M, Leanhardt A E, Raman C, Gustavson T L, Abo-Shaeer J R, Chikkatur A P, Gupta S, Inouye S, Rosenband T and Ketterle W 2001 *Phys. Rev. Lett.* **87** 130402
- [46] Moerdijk A J, Verhaar B J and Axelsson A 1995 *Phys. Rev. A* **51** 4852
- [47] Landau L D 1932 *Phys. Z. Sowjetunion* **2** 46
- [48] Zener G 1932 *Proc. R. Soc. A* **137** 696
- [49] Marder M P 2000 *Condensed Matter Physics* (New York: Wiley) chapter 8
- [50] Wu B and Niu Q 2003 *New J. Phys.* **5** 104
- [51] Blanch G 1964 *Handbook of Mathematical Functions* ed M Abramowitz and I A Stegun (Washington, DC: US Government Printing Office) chapter 20
- [52] Garcia-Ripoll J J and Pérez-García V M 2001 *SIAM J. Sci. Comput.* **23** 1316
- [53] Andrews M R, Mewes M O, van Druten N J, Durfee D S, Kurn D M and Ketterle W 1996 *Science* **273** 84